Influence of Cage Confinement on the Photochemistry of Matrix-Isolated E-beta-Ionone: FT-IR and DFT Study

ARTICLE *in* THE JOURNAL OF PHYSICAL CHEMISTRY A · JANUARY 2013

Impact Factor: 2.69 · DOI: 10.1021/jp310764u · Source: PubMed

3 AUTHORS:

A. Kaczor
Jagiellonian University
64 PUBLICATIONS **541** CITATIONS
SEE PROFILE

Igor D. Reva
University of Coimbra
126 PUBLICATIONS **2,557** CITATIONS
SEE PROFILE

Rui Fausto
University of Coimbra
330 PUBLICATIONS **4,525** CITATIONS
SEE PROFILE

THE JOURNAL OF PHYSICAL CHEMISTRY A

Article

pubs.acs.org/JPCA

Influence of Cage Confinement on the Photochemistry of Matrix-Isolated *E*-β-Ionone: FT-IR and DFT Study

A. Kaczor,*[,†,‡] I. Reva,[§] and R. Fausto[§]

[†]Faculty of Chemistry, Jagiellonian University, Ingardena 3, 30-060 Krakow, Poland

[‡]Jagiellonian Center for Experimental Therapeutics (JCET), Jagiellonian University, Bobrzynskiego 14, 30-348 Krakow, Poland

[§]Department of Chemistry, University of Coimbra, P-3004-535 Coimbra, Portugal

Supporting Information

ABSTRACT: β-ionone, a model compound of carotenoids ring structure, was investigated by FT-IR spectroscopy in a low-temperature argon matrix as well as using B3LYP/6-311++G(d,p) and MP2/6-311++G(d,p) quantum-chemical calculations. The spectrum of matrix-isolated *E*-β-ionone was analyzed and attributed to six conformers of the compound. Then, matrix-isolated *E*-β-ionone was submitted to UV irradiation using either a broadband source (with different cutoff filters) or a narrowband laser/MOPO system (at various wavelengths). Upon 240 nm narrowband irradiation, the formation of both *Z-retro*-γ-ionone and *Z*-β-ionone was observed, the reactant and the photoproducts being in a photostationary equilibrium. Under these conditions, the matrix environment was found to hamper subsequent reactions of *Z-retro*-γ-ionone and *Z*-β-ionone, so that this last species could be observed directly for the first time. Furthermore, the formation of *Z-retro*-γ-ionone was shown to occur directly via an intramolecular [1,5] H-atom shift and thereby, under the constraints imposed by the matrix confinement, the conformations assumed by this photoproduct were found to be strictly determined by those initially assumed by the reactant molecules. Broadband irradiation resulted in the completion of the reaction (disappearance of the reactant) and the sole observation of *Z-retro*-γ-ionone. These results imply that under these conditions the *Z*-β-ionone is unstable, very likely decaying to additional conformers of *Z-retro*-γ-ionone, as reflected in the broader bands due to this photoproduct observed in the infrared spectra of the broadband irradiated matrix.

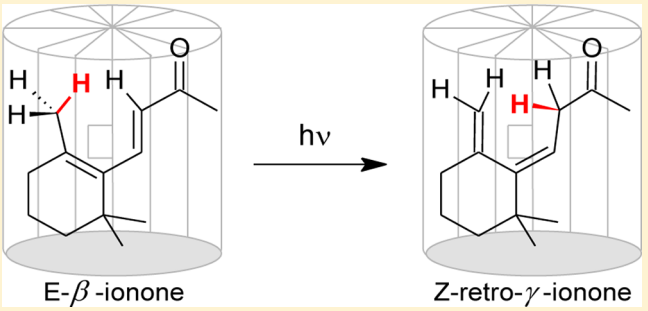

INTRODUCTION

Ionones are a family of terpene compounds of distinct violet, woody odor, with α-ionone being one of the classical odorants introduced by Coty to its perfumes L'Origan as early as in 1906.[1] In nature, ionones are essential oils existing in many plants, such as roses, blackberries, raspberries, black tea, *Osmanthus*, and others.[2−5] The representatives of the ionone family are: *E*-α-ionone [(3*E*)-4-(2,6,6-trimethylcyclohex-2-en-1-yl)but-3-en-2-one], *E*-β-ionone [(3*E*)-4-(2,6,6-trimethylcyclohex-1-en-1-yl)but-3-en-2-one], and *E*-γ-ionone [(3*E*)-4-(2,2-dimethyl-6-methylenecyclohexyl)but-3-en-2-one], differing by the position of one C=C double bond (Scheme 1).

The ionone with the highest conjugation degree, that is, β-ionone, is a building block of all the carotenoids possessing vitamin A activity, including retinal. It was demonstrated that β-ionone activates and bleaches some types of visual pigments in salamander photoreceptors, mimicking the effects of light.[6]

Although the role of the β-ionone ring of retinal in the vision process is not firmly established, it has been shown that there are pronounced interactions between the methyl groups of the β-ionone ring and the retinylidene protein.[7] Early studies have shown that the ring orientation in both β-ionone and retinals should be a "distorted s-cis" conformation around the single bond connecting the unsaturated substituent to the ring, with the respective torsion angle in the 30−70° range.[8] Later, molecular dynamics results carried out on retinals predicted that the β-ionone ring can rotate with some ease relatively to the polyene chain, thereby populating both positively and negatively twisted "s-cis" enantiomers.[9] It was also shown that the twisting of the β-ionone ring relatively to the chain plays an important role in the spectral tuning of retinal in the gas phase.[10]

Scheme 1. Structures of Ionones

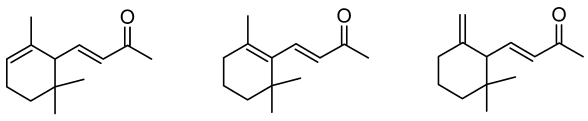

Received: October 31, 2012
Revised: January 9, 2013
Published: January 10, 2013

The β-ionone ring structure was also suggested to play a relevant role in the stabilization of the active state of metarhodopsin II intermediate,[11] the early photoproduct formed as a result of absorption of a photon by retinal and its subsequent cis/trans isomerization. Retinal−protein interactions and the role of the β-ionone ring in the activation of the receptor were verified by high-resolution X-ray crystallography of metarhodopsin II, as reported recently in *Nature*.[12] The 11-cis/trans isomerization of retinal causes elongation of the molecule and clashing of its β-ionone ring between two transmembrane helixes (TM5 and TM6), thus inducing considerable structural changes as well as retinal reorientation.[12] Recent molecular modeling studies on 11-cis-locked retinal analogs in the active site of rhodopsin suggested that the 11-cis/trans isomerization in the native chromophore is probably a mechanism for repositioning of the β-ionone ring, which ultimately leads to helix movements and determines the activation of the receptor.[13] Additional studies indicated that the isomerization of retinal is most probably proceeded by Franck−Condon relaxation involving the β-ionone ring.[14] Density functional theory (DFT) and time-dependent DFT (TD-DFT) calculations suggested that the latter step of the photochemical reaction requires a 60° change in the dihedral angle between the β-ionone ring and the retinal chain, although, according to the authors, this torsional motion may possibly be (at least partially) hindered in the protein rigid environment.[14]

The photochemistry of β-ionone in solution is a fairly well-studied topic (see Scheme 2). Büchi and Yang[15] demonstrated

Scheme 2. Isomerization Pathways of β-Ionone (adapted from refs 21 and 22)

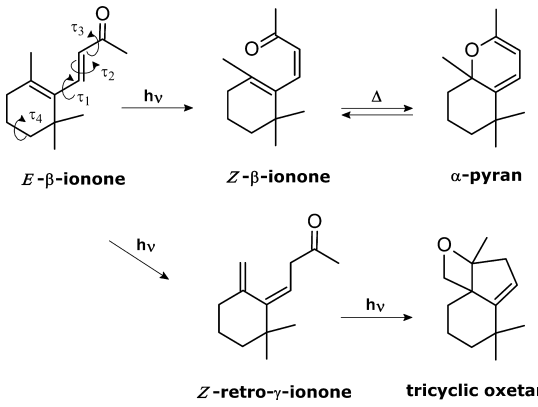

that direct broadband photolysis of *E*-β-ionone in ethanol yields an α-pyran derivative (2,5,5,8a-tetramethyl-6,7,8,8a-tetrahydro-5*H*-1-benzopyran) as the main final product and a byproduct containing a three-membered carbon ring (minor product). The formation of the α-pyran derivative was shown to be a photochemically reversible reaction, proposed to undergo via the *Z*-β-ionone intermediate, which is in the thermal equilibrium with the α-pyran form.[16−18] The isomerization of *E*- to *Z*-β-ionone was suggested to be a triplet reaction, as the triplet-sensitized photolysis of *E*-β-ionone produces the α-pyran derivative as the sole product.[19] This is, indeed, a good example of the general synthetic strategy of preparation of hindered olefins by selective triplet sensitization.[20] Later, it was also demonstrated that at low temperature ($T \leq -50$ °C), where the *Z*-β-ionone→α-pyran thermal reaction is blocked, direct irradiation of *E*-β-ionone in CD_3OD solution in the presence of triplet photosensitizers brings *Z*-β-ionone as the sole product.[19]

Irradiation of *E*-β-ionone in ethanol solution using broadband UV/vis light resulted in the formation of *Z-retro*-γ-ionone (and a tricyclic oxetan secondary product, 6,6,8a-trimethyl-3,4,5,6,8,8a-hexahydroindeno[1,7a-*b*]oxete), apart from the α-pyran derivative[21,22] (see Scheme 2). These main products were also previously proposed by de Mayo et al.[23] The formation of the Z-*retro*-γ-ionone was found to be temperature-independent and blocked in the presence of triplet sensitizers, suggesting that it is produced from an excited singlet state.[21]

It has also been shown that the product distribution in the photochemistry of *E*-β-ionone in solution depends on the presence in the media of electron acceptors, electron donors,[24−26] or other substances, such as, for example, cyclodextrins.[27]

As mentioned, all of the above-mentioned reactions were performed in solution (i.e., in an environment allowing for high rotational freedom) and mostly with the application of UV/vis broadband irradiation. Very interestingly, it was demonstrated that the photochemistry of *E*-β-ionones (e.g., 7-methyl-*E*-β-ionone) may be wavelength-dependent, leading to the *E*-*Z* isomerization upon irradiation at $\lambda > 347$ nm and yielding other products upon irradiation at lower wavelengths, including the photoisomer resulting from the [1,5]-sigmatropic H shift.[28]

To complement the previously described investigations on the photochemistry of *E*-β-ionone, in particular, with the aim to shed light on the photoreactivity of this compound in conditions of restricted movement (i.e., as for carotenoid β-ionone rings in a protein environment, for instance, retinal in metarhodopsin), we decided to perform both narrowband and broadband UV irradiation experiments on *E*-β-ionone isolated in a low-temperature solid argon matrix at 13 to 14 K and follow the progress of the photoinduced reactions using infrared spectroscopy. To help analyzing and interpreting the obtained results, quantum-chemical calculations performed at the MP2/6-311++G(d,p) and DFT(B3LYP)/6-311++G(d,p) levels of theory were employed.

MATERIALS AND METHODS

Experimental Section. *E*-β-ionone ((3*E*)-4-(2,6,6-trimethylcyclohex-1-en-1-yl)but-3-en-2-one, ≥95.0%) was obtained from Fluka (95%) and purified by evaporation.

In the matrix isolation experiments, a glass vacuum system and standard manometric procedures were used to deposit the matrix gas (argon, N60, obtained from Air Liquide). Matrices were prepared by codeposition, onto the cooled CsI substrate of the cryostat, of the matrix gas (argon) and of the compound evaporated from a glass sample compartment connected to the cryostat via a needle valve. During deposition, the temperature of the sample compartment was maintained between 0 and 41 °C and the valve nozzle was kept at 24−41 °C (depending on the experiment). Therefore, it can be approximated that the room temperature defines the equilibrium conformational composition of the deposited compound.

The IR spectra were collected in the 4000−400 cm^{-1} range, with 0.5 cm^{-1} resolution, on a Nicolet 6700 Fourier transform infrared spectrometer equipped with a deuterated triglycine sulfate (DTGS) detector and a Ge/KBr beamsplitter.

All experiments were done on the basis of an APD Cryogenics closed cycle helium refrigeration system with a DE-202A expander. The temperature of the CsI substrate

dx.doi.org/10.1021/jp310764u | *J. Phys. Chem. A* 2013, 117, 888−897

Table 1. Relative Zero-Point-Corrected Energies (ΔE_{corr}, kJ mol^{-1}), Gibbs Free Energies at 298.15 K (ΔG, kJ mol^{-1}), Abundances at 298.15 K (A_{calc}, %), Dipole Moments (μ, debye), and Defining Dihedral Angles (degrees) of *E*-β-Ionone Conformers Calculated at the B3LYP and MP2 Levels of Theory with the 6-311++G(d,p) Basis Set

conformer	ΔE_{corr}[a]	ΔG[b]	A_{calc}[c]	μ	τ_1[c]	τ_2[c]	τ_3[c]
			DFT[d]				
G^+EC	0.00	0.00	30.13	3.81	44.3	178.5	2.4
G^-EC	0.16	0.17	28.15	3.80	−46.1	−178.2	−2.8
TEC	1.98	1.52	16.33	3.75	169.0	−178.4	−1.0
G^+ET	1.63	2.20	12.39	4.41	47.0	179.5	−179.9
G^-ET	2.20	2.78	9.82	4.47	−48.2	−179.2	179.2
TET	5.80	5.58	3.17	5.39	167.6	−178.7	179.4
			MP2[e]				
G^+EC	1.48	0.42	27.34	3.94	51.5	179.1	0.8
G^-EC	2.61	1.39	18.48	3.96	−51.0	−178.0	−2.1
TEC	9.38	7.59	1.52	3.86	167.0	−178.5	−1.7
G^+ET	0.00	0.00	32.43	4.60	52.3	179.9	178.8
G^-ET	1.46	1.30	19.16	4.69	−52.1	−178.9	−179.3
TET	9.22	8.45	1.07	5.69	166.2	−178.8	179.7

[a] E_{corr} = −582.496690 hartree for conformer G^+EC (DFT) and E_{corr} = −580.718467 hartree for conformer G^+ET (MP2). [b] G = −582.539347 hartree for conformer G^+EC (DFT) and G = −580.760907 hartree for conformer G^+ET (MP2) at 298.15 K. [c] Dihedral angles τ_1, τ_2, and τ_3 are defined as (C_1=C_2−C_{11}=C_{13}), (C_2−C_{11}=C_{13}−C_{15}), and (C_{11}=C_{13}−C_{15}=O_{34}), respectively (see Figure 1 for atom numbering). [d] B3LYP/6-311++G(d,p). [e] MP2/6-311++G(d,p); all structures have C_1 symmetry.

during deposition was 13 to 14 K. Necessary modifications of the sample compartment of the spectrometer were made to accommodate the cryostat head and allow efficient purging of the instrument by a stream of dry air to remove water and CO_2 vapors.

Annealing of the matrix with the deposited *E*-β-ionone was performed by increasing the temperature of the matrix from 13 to 27 K. The spectra were registered in this temperature range after every 2° of temperature increase.

The selective UV irradiation was carried out with pulsed narrowband UV radiation (240 or 290 nm). It was generated by the third harmonic of a Nd:YAG Quanta-Ray PRO-230-10 pump laser (355 nm) and converted to the used UV frequency output (fwhm ∼0.2 cm^{-1}) by an optical parametric oscillator (Spectra-Physics MOPO SL, with IEE-488 and MAP-SL options) coupled to a frequency-doubling module FDO-970. The output pulses, having energy of ∼1 mJ and repetition rate of 10 Hz, were directed to the sample via an external quartz window of the cryostat. Alternatively, the matrices were irradiated through the outer KBr window (cutoff ∼235 nm) of the cryostat or Pyrex filter (cutoff ∼290 nm) with light from a 500 W Hg(Xe) lamp (Spectra-Physics, model 66142), adjusted to provide an output power in the range of 175−200 W.

In the course of the experiments, the temperature of the matrices was measured directly at the sample holder by a silicon diode sensor connected to a digital controller (Scientific Instruments, model 9650−1) and did not exceed 14 K.

Computational. The quantum chemical calculations were performed with Gaussian 03 (Gaussian, revision E.01)[29] or Gaussian 09 (revision A.02)[30] at the DFT level of theory, using the 6-311++G(d,p) basis set. The DFT calculations were carried out with the three-parameter density functional abbreviated as B3LYP, which includes Becke's gradient exchange correction,[31] the Lee, Yang, and Parr correlation functional,[32] and the Vosko, Wilk, and Nusair functional.[33]

Potential energy profiles for internal rotation defined by the τ_1 torsional coordinate (see Scheme 2) for both *E*- and *Z*-β-ionone were calculated at the B3LYP/6-311++G(d,p) level, performing relaxed scans on the corresponding potential energy surface (PES) for all possible combinations of cis and trans conformations of τ_2 and τ_3 coordinates.

The minima found on *E*- and *Z*-β-ionone PES were subsequently fully optimized, and the vibrational frequencies were calculated for the fully optimized structures. The structures of the probable photoproducts were computed at the same theory level. The optimized geometries of β-ionone conformers and photoproducts were confirmed to correspond to true minimum energy conformations by inspection of the corresponding calculated Hessian matrices. Calculations on β-ionone conformers were additionally carried out at the MP2 level[34−39] with the same basis set.

The transition-state structures for conformational interconversions were obtained using the synchronous transit-guided quasi-Newton (STQN) method.[40,41]

The DFT-calculated harmonic frequencies were used in the analysis of the experimental spectra. They were scaled down to account mainly for anharmonicity effects and limitations of the basis set. The scaling factor of 0.978 for B3LYP/6-311++G(d,p) was adopted from previous works.[42−44] Potential energy distributions (PEDs) in terms of natural internal coordinates[45] were computed with the GAR2PED program.[46]

RESULTS AND DISCUSSION

β-Ionone Structures. Scheme 2 shows the four internal torsional coordinates that provide structural multiplicity in β-ionone. The structures differing by orientation around the exocyclic C=C bond (τ_2) give rise to two isomeric varieties, E and Z. They should exist at room temperature as two independent compounds. Indeed, as indicated in the Experimental Section, more than 95% of the β-ionone sample studied in this work was the E-isomer.

The three dihedral angles (Scheme 2, Table 1), τ_1, τ_3, and τ_4, corresponding to internal rotations around single bonds, give rise to different conformers of *E*-β-ionone. All conformers belong to the C_1 point group and are doubly degenerate by symmetry, whereas half of the conformers are mirror images of the other half, having the same absolute values of dihedral

dx.doi.org/10.1021/jp310764u | J. Phys. Chem. A 2013, 117, 888−897

angles and opposite signs. Also, it is interesting to note that all conformers can be divided in two families, differing by the τ_4 dihedral, either having the "gauche plus" or "gauche minus" ring arrangement. Such ring configurations are typical of molecules based on cyclohexene moiety.[47] If the ring configuration is arbitrarily fixed into one of the two possible values, then the variation of the two remaining dihedral angles will describe all unique possible conformers of the system. Thus, only the family with τ_4 around +60° is considered hereafter because the other family (with τ_4 being ca. −60°) consists of mirror images of the former family. Combinations of the remaining two dihedral angles, τ_1 and τ_3, result in six unique structures of *E*-*β*-ionone.

In the naming system adopted here, the first, second, and third letters denote the conformation/configuration with respect to the τ_1, τ_2, and τ_3 dihedral angles, respectively. G^+, G^-, *E*, *Z*, *C*, and *T* designate gauche plus, gauche minus, entgegen, zusammen, cis, and trans arrangements, respectively. The corresponding structures optimized at the B3LYP level are shown in Figure 1.

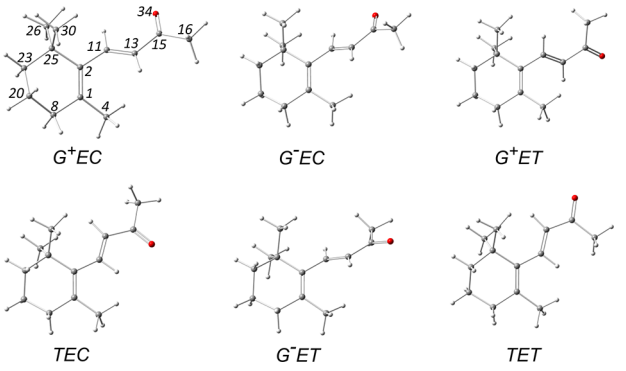

Figure 1. Six unique *E*-*β*-ionone conformers optimized at the B3LYP/6-311++G(d,p) level of theory with the adopted numbering scheme for non-hydrogen atoms.

Previously, we have shown that the MP2 in general outperforms the B3LYP method regarding the prediction of relative stabilities for conformationally flexible molecules.[48−50] In several cases, it was possible to compare the theoretically predicted relative energies with the relative energies obtained experimentally.[49,51,52] In all of these cases, the MP2 energy prediction was closer to the experiment than the B3LYP. That is why in the present study we carried out calculations of the relative conformational stabilities at both the MP2 and DFT levels.

The values of zero-point-corrected energies and Gibbs free energies of *E*-*β*-ionone, as well as their expected abundances at room temperature, are given in Table 1. The conformers in this Table are organized into two families, *XEC* and *XET*, where *X* adopts all possible values (G^+, G^-, and *T*). It is interesting to note the calculated relative stabilities of these forms. Within each family, the stability decreases in the sequence $G^+ > G^- \gg T$. Across families (in the pairs with the same *X*), the *XEC* forms are always more stable than *XET*, by 1 to 2 kJ mol^{-1} at the DFT level. At the MP2 level, inversely, the *XET* forms are predicted to be more stable by nearly the same gap. Overall, all of the conformers with $X = G^{\pm}$ fall in a narrow margin of stabilities (0−3 kJ mol^{-1}) and are expected to be significantly populated at room temperature.

The structures with the cis arrangement around τ_1 were predicted to be transition-state structures of the first order and not minima on the PES. The low-energy forms found in this work are in agreement with the minima presented by Legnani et al.,[53] computed at a lower theory level (B3LYP/6-31G(d)). According to our calculations, the same six structures constitute the whole population of *E*-*β*-ionone at room temperature. The defining dihedral angles of *E*-*β*-ionone conformers are shown in Table 1. It is interesting to note that the MP2 calculated values of dihedral angle τ_1 show larger deviations from planarity (larger numeric values) for $X = G^{\pm}$ compared with the calculations of the same structures at the DFT level. This is due to the fact that MP2 calculations better describe the noncovalent interactions existing in the studied molecules. Furthermore, the arrangement of the dihedral angle τ_1 influences the $C_1{=}C_2$ and $C_2{-}C_{11}$ bond lengths (Table S1, Supporting Information). The $G^{\pm}$ is the preferred arrangement of the τ_1 angle, as it implies the lack of the steric hindrance present in *T* structures due to presence of heavy and bulky substituents "on the same side" of the double bond. The calculations predict that *T* forms correspond to <20% (DFT) or <3% (MP2) of the total conformational equilibrium (see Table 1). The $G^{\pm}$ arrangement of the C=C bonds of the *β*-ionone rings is predicted to be the preferred one also for carotenoids in the gas phase.[54−56] As it will be shown below, the $G^{\pm}$ forms (around τ_1) dominating in *E*-*β*-ionone are precisely the forms responsible for the typical photochemistry observed in this study.

IR Spectrum of *β*-Ionone in the Low-Temperature Matrix. The fingerprint range of the spectrum of *E*-*β*-ionone isolated in the low-temperature Ar matrix is presented in Figure 2, along with the sum-spectrum obtained by adding the spectra of the six most stable forms of the compound scaled by their abundances (Table 1). Contributions of the two families to the simulated spectra are shown by distinct colors, blue (*XEC*) and red (*XET*). Figure 2 also shows two different types of simulation. In one of them, the weighting factor for calculated intensities is derived from the DFT calculations (Figure 2, bottom), whereas in the second it is obtained from the MP2 calculations (Figure 2, top). The latter approach was adopted from one of our previous studies.[57]

The comparison between the experimental and computed sum-spectra allows separating between the contributions of *XET* versus *XEC* type forms present in the matrix. This can be followed by analysis of some characteristic absorptions, for example, the pairs of bands at 1707/1683 and 1252/918 cm^{-1} (middle frame, Figure 2). The bands assigned to *XET* forms exhibit higher intensities relative to those due to *XEC* conformers than it could be expected from the DFT computations. The intensity ratios in these pairs of bands show that the DFT calculations underestimate the stability of *XET* relative to *XEC* forms, whereas the MP2 seems to slightly overestimate this relative stability.

The theoretical spectra of single conformers are given in Figure S1 (Supporting Information). The definition of the internal coordinates used in the normal modes analysis of *E*-*β*-ionone and the detailed assignment of the bands are given in Tables S2 and S3 (Supporting Information). Here the attention of the reader is directed toward absorptions that allow for distinguishing between different groups of conformers, that is, marker bands for different groups of forms.

The first group of bands, at ca. 1707 and 1683 cm^{-1} (the latter with a shoulder at ca. 1669 cm^{-1}), assigned to the *ν*C=O

dx.doi.org/10.1021/jp310764u | J. Phys. Chem. A 2013, 117, 888−897

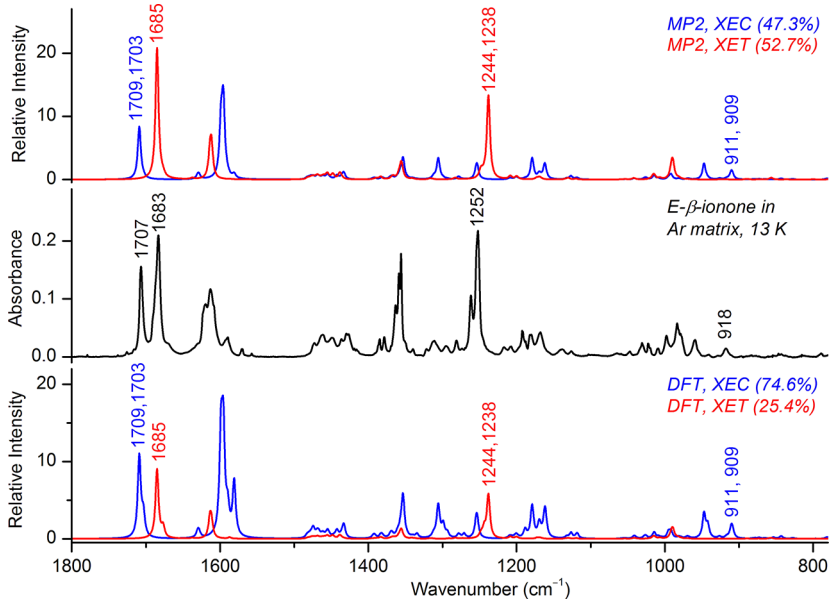

Figure 2. Experimental FT-IR spectrum of matrix-isolated *E*-*β*-ionone (middle, black), compared with theoretical spectra of *E*-*β*-ionone conformers belonging to the *XEC* (blue) and *XET* (red) families calculated at the B3LYP level of theory. Theoretical intensities were multiplied by predicted equilibrium populations of the corresponding forms estimated using the DFT (bottom) and MP2 (top) calculated Gibbs free energies at 298 K. (See Table 1.) Theoretical spectra were broadened by Lorentzian profiles having fwhm of 5 cm^{-1} and centered at the calculated frequencies scaled by 0.978.

stretching vibrations, allows for differentiating between *XEC* and *XET* isomers. The bands due to this vibration are, according to the computations, placed at higher wavenumbers for *XEC* forms (calc: 1709, 1703, 1685, and 1677 cm^{-1} for $G^{\pm}EC$, *TEC*, $G^{\pm}ET$, and *TET*, respectively). This is in agreement with the predicted C═O bonds lengths, calculated to be longer by ∼0.3 pm in the *XET* forms, compared with the *XEC* forms.

Also, the frequency of the band with 21−39% PED contribution from the $\nu C_{13}-C_{15}$ vibration is diagnostic for distinguishing between *XEC* and *XET* forms. Both B3LYP and MP2 computations predict the $C_{13}-C_{15}$ bond to be 0.6 to 1 pm shorter in the *XET* structures than in the *XEC* ones. This bond shortening brings a considerable difference in the wavenumber of the bands related with vibrations of this fragment. In the case of the *XET* minima, the bands with ca. 31−39% contribution of this coordinate are expected to occur at 1244 and 1238 cm^{-1} for *TET* and $G^{\pm}ET$ forms, respectively, and were observed experimentally as a strong band at ca. 1252 cm^{-1}. For *XEC* forms, absorptions with 21−25% contribution from this coordinate are predicted at 911 and 909 cm^{-1} for $G^{+}EC$ and $G^{-}EC$, respectively, and are observed in the matrix-isolation spectrum at 918 cm^{-1}. Also, the intensity of this band is significantly larger for *XET* forms, even accounting for their considerably smaller abundance (overall ∼25%) relative to *XEC* forms. Therefore, the absorptions involving the $C_{13}-C_{15}$ stretching vibration are very suitable marker bands to distinguish between these two groups of forms (*XEC* vs *XET*).

The marker region to discern between the $G^{\pm}XX$ and *TXX* forms is more difficult to establish, as the absorptions related to the C_2-C_{11} stretching vibration are of low intensity and, additionally, they have only small contributions from this mode (9−18%, exp: 1138 and 1126 cm^{-1}, calc: 1132−1118 cm^{-1}). In turn, the absorptions with the highest contribution from the $\nu C_1{=}C_2$ mode are overlapped with the bands due to $\nu C_{11}{=}C_{13}$ vibrations and therefore their exact assignment is difficult. Nevertheless, it is possible to note that the experimental bands observed at 1613 and 1589 cm^{-1} are related mostly to the C═C stretching vibrations of $G^{\pm}EC$ and *TEC* forms, respectively. Finally, no proper marker region could be identified to distinguish between $G^{\pm}ET$ and *TET* conformers due to the small abundance of the latter form. A summary with the identified marker bands is given in Table 2.

Table 2. Marker Bands in the IR Spectra of Matrix-Isolated *E*-*β*-Ionone at 13 K

experimental	calculated[a]		
ν_{exp} [cm^{-1}]	ν_{calc} (cm^{-1}) (I [km mol^{-1}])	conformer(s)	approximate assignment
1707	1709(83.7), 1703 (21.9)	***XEC***	$\nu C_{15}{=}O_{34}$ (68−70)[b]
1683	1685(109.8)	***XET***	$\nu C_{15}{=}O_{34}$ (80)[b]
1613	1599(95.5), 1596(100.5)	$\boldsymbol{G^{\pm}EC}$	$\nu C{=}C$ (55)[b]
1589	1590(24.3), 1581(55.5)	***TEC***	$\nu C{=}C$ (49−61)[b]
1252	1244(9.0), 1238(45.2)	***XET***	$\nu C_{13}-C_{15}$ (31−39)[b,c]
918	911(8.2), 909(7.9)	$\boldsymbol{G^{\pm}EC}$	$\nu C_{13}-C_{15}$ (21−25)[b,c]

[a]B3LYP/6-311++G(d,p); frequencies scaled by the factor of 0.978; intensities scaled by the calculated abundance of conformers (see Table 1). [b]PED contribution (in %) of the listed vibration. [c]It is necessary to underline that $\nu C_{13}-C_{15}$ has only 21−39% contribution in the described mode, which overall is qualitatively different for both groups of forms.

Photochemistry of *E*-*β*-Ionone Confined in the Matrix Cage. Irradiation of matrix-isolated *E*-*β*-ionone with λ = 240 nm (5 mW) monochromatic light results in isomerization of the compound into *Z*-*retro*-*γ*-ionone and *Z*-*β*-ionone (Figure 3). No subsequent photoreactions of these products (for instance to the oxetan or *α*-pyran derivatives shown in Scheme

dx.doi.org/10.1021/jp310764u | J. Phys. Chem. A 2013, 117, 888−897

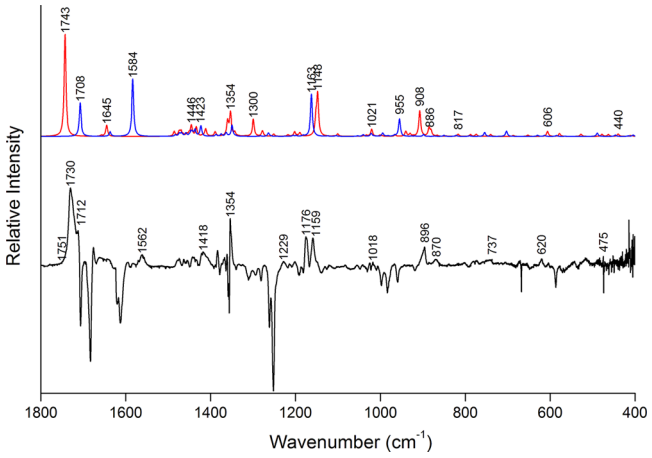

Figure 3. Theoretical spectrum of *Z-retro-γ*-ionone ($G^{-}Ac^{-}Ac^{-}$ conformer, red line) and *Z-β*-ionone ($G^{+}ZT$ conformer, blue line) in the 1:0.5 ratio, respectively, and FT-IR spectrum obtained by subtraction of the spectrum of matrix-isolated *E-β*-ionone (Ar, 14K) from the spectrum after irradiation with 240 nm light for 270 min (black line). Theoretical spectra have been broadened by a Lorentzian having a width of 5 cm^{-1}.

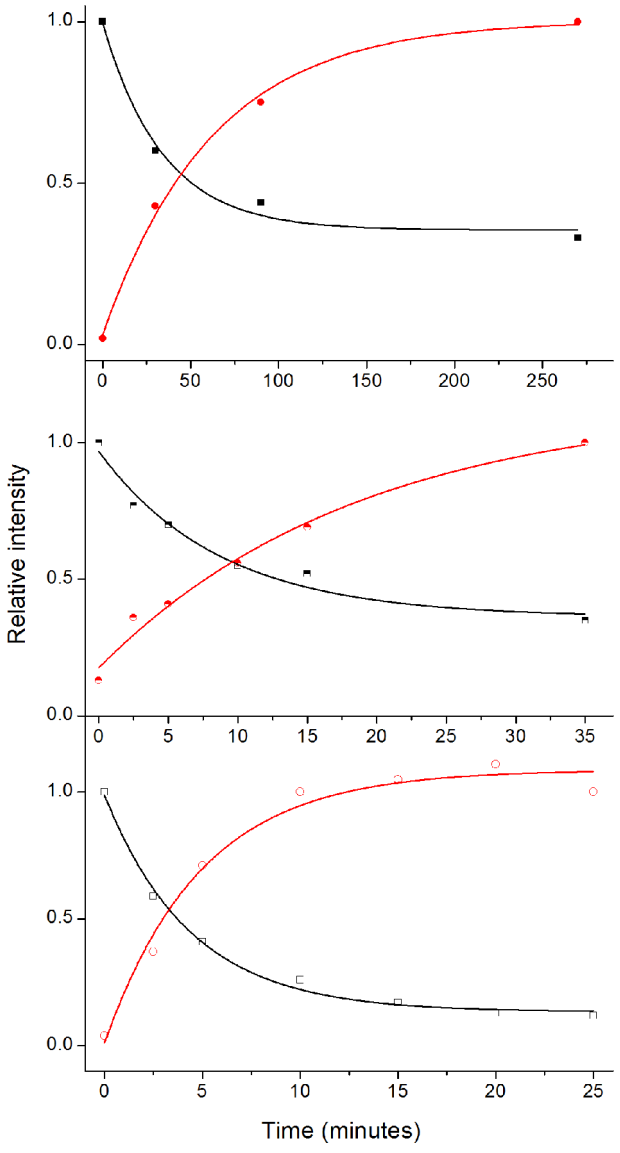

Figure 4. Change with time of irradiation: laser light, λ = 240 nm (upper panel), broadband irradiation λ > 290 nm (middle panel), and λ > 235 nm (bottom panel) of matrix-isolated *E-β*-ionone (black squares) and the observed photoproduct of reaction assigned to *Z-retro-γ*-ionone (red circles). Squares: average of three well-defined bands (at 918 (only for λ = 240 nm), 1252, and 1262 cm^{-1}). Circles: average of two well-defined bands (at 895 and 1730 cm^{-1}). The intensity for the substrate and the product was normalized to unity for 0 and 270 min, respectively.

2) were observed. Because a significant number of bands due to the reactant and products overlap, the *E-β*-ionone spectrum was subtracted from the spectrum registered after 270 min of irradiation (Figure 3b) and then compared with the B3LYP/6-311++G(d,p) simulated spectra of the mentioned photoproducts.

The amount of *Z-retro-γ*-ionone (red line, Figure 4, upper panel) continuously increased during 270 min of irradiation of the matrix at the expense of an exponential decay of *E-β*-ionone. The kinetics of *Z-β*-ionone production could not be evaluated due to the fact that the bands due to this photoproduct overlap strongly with *E-β*-ionone absorptions.

As shown in the previous section, more than 80% (97% if MP2 data are taken into account; see Table 1) of the starting compound assumes either the G^{+} or G^{-} orientation about τ_1 in the room temperature gas-phase equilibrium mixture of *E-β*-ionone conformers. This is equivalent to say that the methyl group of the ring (at the C_4 atom) is in the closest spatial vicinity regarding the exocyclic C═C bond; more precisely, it is placed close to the C_{13} atom. Under such conditions, the hydrogen atoms of the C_4-based methyl group are prepared for an intramolecular [1,5]-hydrogen shift to C_{13}. If such a hydrogen shift occurs, then the resulting structure would be *Z-retro-γ*-ionone. This H-atom migration can be expected to be even more favorable in excited states where the C_{11}−C_{13} bond loses its double-bond character and the substituents at this bond assume a nearly perpendicular configuration. Such configuration may also be related to the E-Z isomerization around this bond, which converts *E-β*-ionone into *Z-β*-ionone and vice versa. In this case, we can also expect that the [1,5]-hydrogen shift reaction can also be efficient for the G^{+} and G^{-} τ_1 conformers of *Z-β*-ionone.

The archetype reaction for this sort of isomerization has been known since the 1960s and reported originally by Roth and König[58] for the prototype molecule 1,3-pentadiene. This reaction has been explored subsequently in many theoretical and experimental studies. Surprisingly, the large kinetic isotope effect, reported by Roth and König,[58] has been explained by Dewar et al.[59,60] to be related to vibrationally assisted tunneling (VAT). This suggestion has been confirmed by other works; for example, Chantranupong and Wildman predicted theoretically the VAT [1,5] H-shift in the s-cis conformer of 1,3-*Z*-pentadiene (a higher-energy form compared with s-trans).[61]

Additionally, phenyl substituents in substituted 1,3-*Z*-pentadienes were demonstrated computationally to reduce the activation enthalpy for [1,5]-hydrogen shift thermal isomerization in these molecules.[62,63] The characteristic of the system is that the two carbon atoms involved in the H-atom shift exchange their hybridization states (sp^2 and sp^3) and the reaction can occur in both directions. This means that the most probable outcome of such reaction would be the establishment of a photoequilibrium, where a prolonged irradiation would stabilize the amounts of the *β*-ionones (E and Z) and *Z-retro-γ*-

dx.doi.org/10.1021/jp310764u | J. Phys. Chem. A 2013, 117, 888−897

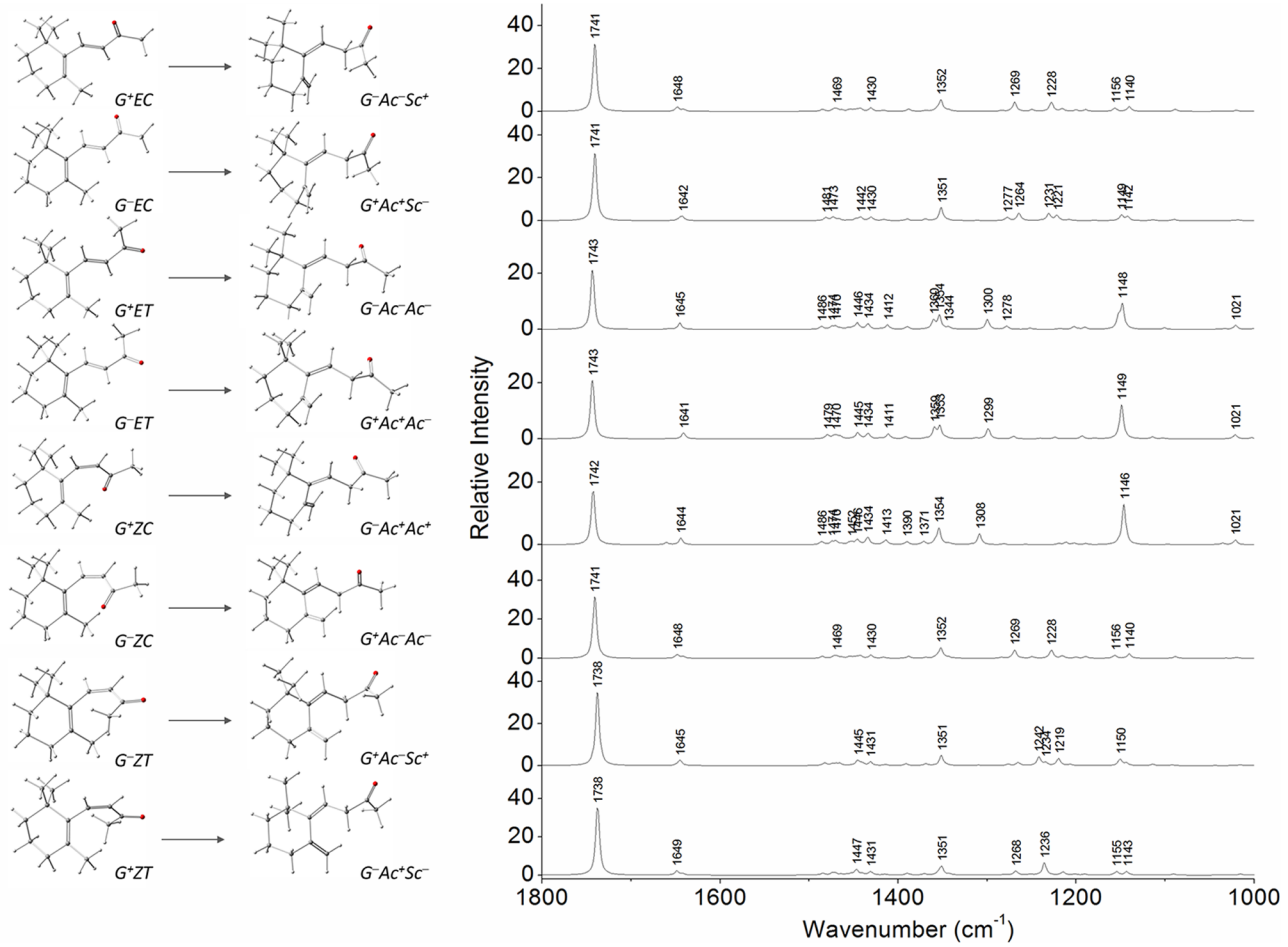

Figure 5. Theoretical spectra of most probable *Z-retro-γ*-ionone forms (right panel) with the optimized geometries of the respective forms (middle panel) and the geometries of the corresponding reactant species (left panel). Theoretical spectra have been broadened by a Lorentzian having a width of 5 cm^{-1}.

ionone to a constant level. Indeed, such behavior was observed in our selective wavelength experiment (see Figure 4, upper panel). Therefore, the intramolecular H-atom shifts leading from *G*-type forms of *E*- and *Z-β*-ionone to *Z-retro-γ*-ionone were simulated in this study theoretically for all four *G*-type conformers of *E-β*-ionone as well as for the four *G* conformers of *Z-β*-ionone (the latter presented in Table S4 and Figure S2, Supporting Information). These simulations permitted us to establish the conformational arrangements of the resulting *Z-retro-γ*-ionone, which are depicted in Figure 5 along with their simulated spectra.

One of the characteristics of *Z-retro-γ*-ionone is the shift of the double bond to outside the six-membered ring. The new ring becomes completely saturated (as in cyclohexane) and can adopt different conformations (chair-ring and twist-ring). In the course of the simulations of the hydrogen atom shifts, we found that on four occasions the resulting *Z-retro-γ*-ionone product adopts the chair-ring conformation, whereas in the other four cases the hydrogen shift leads to a twist ring. Whereas in the gas phase the chair conformation should be strongly preferred on energetic reasons, in the matrix rigid environment, the product is most often geometrically similar to its precursor due to locking of the precursor in the matrix cage (nonequilibration of excited rotamers principle, NEER, verified originally for matrix-isolated 1,3,5-hexatriene).[64]

The spectra of those *Z-retro-γ*-ionone forms that could be formed as a result of [1,5]-H-shift are quite similar (Figure 5), a number of weak-to-medium intensity features and the intense band at ca. 1740 cm^{-1} due to the carbonyl stretching vibration fitting well to the broad feature observed in the experimental spectrum at ca. 1730 cm^{-1}. Because this absorption is predicted at nearly the same frequency in all forms (1738−1748 cm^{-1}), it does not allow distinguishing between conformers. The presence of an experimental intense band at 1159 cm^{-1} (see Figure 3) allows for concluding that at least one of the following forms: $G^-Ac^-Ac^-$, $G^+Ac^+Ac^-$, and $G^-Ac^+Ac^+$, has to be produced (to describe forms, three dihedrals are given: $C_4{=}C_1{-}C_2{=}C_{11}$ (τ_1'), τ_2, and τ_3, respectively; *Ac* and *Sc* denote anticlinal and synclinal arrangements, respectively; see Figure 5). Indeed, in all three mentioned forms a medium-intensity band is predicted to occur around 1150 cm^{-1}. The common feature of these three forms is the anticlinal (and close to trans) arrangement of the τ_3 dihedral. The $G^-Ac^-Ac^-$ form was chosen to account for *Z-retro-γ*-ionone formation in Figure 3. The choice of this form is justified by the fact that its expected *E-β*-ionone precursor should be the G^+ET form, which is the most stable (and consequently the most populated) among all *E-β*-ionone conformers according to the MP2 calculations (see Table 1).

There are several features in the experimental spectrum that cannot be assigned to *Z-retro-γ*-ionone, particularly the

dx.doi.org/10.1021/jp310764u | J. Phys. Chem. A 2013, 117, 888−897

shoulder at ca. 1712 cm^{-1} and the bands at 1562 and 1176 cm^{-1}. On the basis of previously considered photoreaction pathways[16−18] and the present quantum-chemical computations, these bands are assigned here to *Z*-*β*-ionone.

The spectra of four *Z*-*β*-ionone conformers are given in Figure S2 (Supporting Information), which demonstrates that only two of these forms (namely, G^+ZT and G^-ZT) fit the profile of the product bands not ascribable to *Z*-*retro*-*γ*-ionone. The vibrational signatures of both G^+ZC and G^-ZC exclude their presence in the spectra of the irradiated samples. Because the G^+ZT and G^-ZT spectra are nearly identical, the former was chosen to show *Z*-*β*-ionone formation in Figure 3. According to our knowledge, *Z*-*β*-ionone was for the first time *directly* observed in the present study.

Note that in both cases, that is, *Z*-*retro*-*γ*- and *Z*-*β*-ionone, a conformation close to *trans*-τ_3 is preserved in the photoproducts, suggesting that rotation around τ_3 faces steric hindrance disabling or hampering the reaction toward conformers of type cis (for *Z*-*β*-ionone) or synclinal (for *Z*-*retro*-*γ*-ionone).

A distinguishable characteristics of the performed photochemical narrowband and broadband experiments is that whereas in the first ones a photoequilibrium is established in the system between *E*-*β*-ionone, *Z*-*retro*-*γ*-ionone (Figure 4, upper panel), and, likely, *Z*-*β*-ionone, in the case of the broadband irradiation experiments (Figure S3, Supporting Information), the *Z*-*β*-ionone is not observed. This result suggests that *Z*-*β*-ionone, once formed, is quickly consumed upon broadband irradiation, likely producing additional conformers of *Z*-*retro*-*γ*-ionone, which also justifies the fact that the bands due to *Z*-*retro*-*γ*-ionone are considerably broader in the spectra resulting from broadband irradiation compared to narrowband excitation. Additionally, upon broadband irradiation with $\lambda > 290$ nm, at similar concentration of the photoproduced *Z*-*retro*-*γ*-ionone as that resulting from the narrowband irradiation, no photoequilibrium was established between this species and the reactant (Figure 4, upper panel), and, for irradiation with $\lambda > 235$ nm, the reaction is practically completed (Figure 4, bottom panel).

CONCLUSIONS

The τ_1 torsional coordinate preference for a gauche arrangement was shown previously for carotenoids of various chain lengths and in various environments.[65] This arrangement is also preferred for *β*-ionone in the argon matrix rigid environment. In agreement with the experimental results, calculations predict that τ_1 adopts a gauche geometry in more than at least 80% of the conformational population of *β*-ionone at room temperature. Apparently, the length of the chain does not significantly influence the τ_1 conformation. For native 11-cis retinal chromophore embedded in rhodopsin, calculations predict that in the ground state of the preferred form τ_1 is equal to −39°.[14]

Upon selective 240 nm excitation, decrease in the *E*-*β*-ionone bands and simultaneous increase in absorptions assigned to both *Z*-*β*-ionone and *Z*-*retro*-*γ*-ionone are observed in the approximate ratio of 0.5:1. Based on computational models of possible forms of *Z*-*retro*-*γ*-ionone obtained after [1,5]-hydrogen shift from both *β*-ionone geometric isomers (E and Z), it was possible to determine the conformation of τ_3 in both *Z*-*β*- and *Z*-*retro*-*γ*-ionone in the photolyzed matrices. The close-to-trans arrangement of τ_3 in the photoproducts is determined by the movement constraints existing in the low-temperature matrix environment. Additionally, the gauche conformation of τ_1 in the photoproducts results most probably from the fact that only the gauche τ_1 conformers of *β*-ionone are photoreactive. According to our knowledge, the formation of *Z*-*β*-ionone is for the first time shown explicitly in the present study via its infrared signature.

Photoproduction of *Z*-*retro*-*γ*-ionone is shown to achieve a plateau after ca. 270 min of narrowband irradiation (λ = 240 nm) when ∼60% of the substrate is consumed (Figure 4, upper panel). Analysis of the photoproducts obtained upon broadband excitation (Figure S3 of the Supporting Information) shows that, in this case, splitting and broadening of bands due to the *Z*-*retro* product is observed along with complete consumption of the substrate. This indicates that in the case of broadband excitation there is an alternative source of *Z*-*retro*-*γ*-ionone leading to different conformers of the compound. Most probably, these other forms of *Z*-*retro*-*γ*-ionone are obtained via Z-*β*-ionone → *Z*-*retro*-*γ*-ionone photoisomerization, which was suggested previously from indirect evidence.[19] The reactivity of *Z*-*β*-ionone was found to be wavelength-dependent. For the narrowband 240 nm excitation, the photoproduced ionones exist in equilibrium; therefore, *E*-*β*- and *Z*-*β*-ionone are not fully consumed (a plateau is reached in the kinetic plots after 270 min of the λ = 240 nm irradiation), whereas for broadband irradiation with the 235 nm cutoff filter, *E*-*β*-ionone is practically fully isomerized to the *Z*-*retro* form after a few minutes of irradiation, and *Z*-*β*-ionone is not visible in the spectra since the onset of the reaction.

The major difference in the reaction progress for matrix-isolated *E*-*β*-ionone, compared with reactions in solution, is the lack of any secondary photoproducts obtained from the species produced in the primary photoreactions (i.e., *Z*-*β*-ionone and *Z*-*retro*-*γ*-ionone), particularly the isomeric *α*-pyran observed together with or instead of *Z*-*β*-ionone.[19,21,66,67] The fact that in solution *Z*-*β*-ionone exists in thermal equilibrium with its isomeric *α*-pyran was the condition disabling direct observation of *Z*-*β*-ionone up to now. The indirect evidence of its formation from *E*-*β*-ionone as a primary product was possible in the past due to the fact that below 50 °C interconversion of *Z*-*β*-ionone to the *α*-pyran is fully inhibited.[19] In the matrix, however, the conversion of *Z*-*β*-ionone toward the *α*-pyran does not occur, most probably due to both steric confinement of *Z*-*β*-ionone in the argon cage and lack of thermal energy at 14 K. Conversion of *Z*-*β*-ionone into the *α*-pyran product would require significant reorganization of the *Z*-*β*-ionone chain that is considerably hampered in the rigid environment of solid argon. For the same reason, the *Z*-*retro*-*γ*-ionone → oxetan isomerization is not observed.

The obtained data then clearly show that the rigid environment significantly affects the photoreactivity of *E*-*β*-ionone by blocking ring cyclization reactions observed commonly in solution.[19,21,66,67] This restriction of movement together with the selectivity achieved upon narrowband excitation of matrix-isolated *E*-*β*-ionone led to the possibility of direct observation of the otherwise unstable *Z*-*β*-ionone that in other circumstances promptly isomerizes to *Z*-*retro*-*γ*-ionone or to the previously observed *α*-pyran derivative. The discussion of the mechanisms by which different excitation conditions open different reaction pathways deserves further studies. The TDDFT calculations show that *β*-ionones have several excited electronic states in the 210−370 nm range.[68] However, the mechanistic insight is not trivial because "the link

between structure and vertical theoretical spectrum may be ambiguous".[68]

■ ASSOCIATED CONTENT

Supporting Information

Geometric parameters for the six conformers of *E*-β-ionone calculated at the B3LYP/6-311++G(d,p) level. Definition of internal coordinates used in the normal modes analysis of β-ionone. Assignment of the fingerprint region of FT-IR spectrum of β-ionone in Ar matrix at 13 K. Harmonic frequencies and intensities calculated at the B3LYP/6-311++G(d,p) level. Relative zero-point-corrected energies, Gibbs free energies at 298.15 K, abundances at 298.15 K, dipole moments, and defining dihedral angles of *Z*-β-ionone conformers calculated at the B3LYP/6-311++G(d,p) level of theory. Theoretical IR spectra of *E*-β-ionone conformers (B3LYP/6-311++G(d,p)). Optimized geometries and theoretical IR spectra of *Z*-β-ionone conformers (B3LYP/6-311++G(d,p)) along with their optimized geometries. FT-IR spectrum of matrix-isolated β-ionone after 20 min of broadband irradiation and FT-IR spectrum obtained by subtraction of matrix-isolated β-ionone from the spectrum after irradiation with 240 nm light for 270 min. This material is available free of charge via the Internet at http://pubs.acs.org.

■ AUTHOR INFORMATION

Corresponding Author

*E-mail: kaczor@chemia.uj.edu.pl.

Notes

The authors declare no competing financial interest.

■ ACKNOWLEDGMENTS

This study was supported by the Polish Ministry of Science and Higher Education (grant no. 204311037, 2009-2012). Academic Computer Centre *Cyfronet* is acknowledged for computing time. This research was supported in part by PL-Grid Infrastructure.

■ REFERENCES

(1) Kraft, P.; Bajgrowicz, J. A.; Denis, C.; Frater, G. *Angew. Chem., Int. Ed.* **2000**, *39*, 2981.
(2) Du, X. F.; Finn, C. E.; Qian, M. C. *Food Chem.* **2010**, *119*, 1127.
(3) Du, X. F.; Kurnianta, A.; McDaniel, M.; Finn, C. E.; Qian, M. C. *Food Chem.* **2010**, *121*, 1080.
(4) Wang, L. M.; Li, M. T.; Jin, W. W.; Li, S.; Zhang, S. Q.; Yu, L. J. *Food Chem.* **2009**, *114*, 233.
(5) Werkhoff, P.; Bretschneider, W.; Guntert, M.; Hopp, R.; Surburg, H. *Z. Lebensm.-Unters. Forsch.* **1991**, *192*, 111.
(6) Isayama, T.; England, S. L. M.; Crouch, R. K.; Zimmerman, A. L.; Makino, C. L. *Visual Neurosci.* **2009**, *26*, 267.
(7) Creemers, A. F. L.; Kiihne, S.; Bovee-Geurts, P. H. M.; DeGrip, W. J.; Lugtenburg, J.; de Groot, H. J. M. *Proc. Natl. Acad. Sci. U.S.A.* **2002**, *99*, 9101.
(8) Honig, B.; Hudson, B. D.; Sykes, B. D.; Karplus, M. *Proc. Natl. Acad. Sci. U.S.A.* **1971**, *68*, 1289.
(9) Lau, P. W.; Grossfield, A.; Feller, S. E.; Pitman, M. C.; Brown, M. F. *J. Mol. Biol.* **2007**, *372*, 906.
(10) Cembran, A.; Gonzalez-Luque, R.; Altoe, P.; Merchan, M.; Bernardi, F.; Olivucci, M.; Garavelli, M. *J. Phys. Chem. A* **2005**, *109*, 6597.
(11) Bartl, F. J.; Fritze, O.; Ritter, E.; Herrmann, R.; Kuksa, V.; Palczewski, K.; Hofmann, K. P.; Ernst, O. P. *J. Biol. Chem.* **2005**, *280*, 34259.
(12) Choe, H. W.; Kim, Y. J.; Park, J. H.; Morizumi, T.; Pai, E. F.; Krauss, N.; Hofmann, K. P.; Scheerer, P.; Ernst, O. P. *Nature* **2011**, *471*, 651.
(13) Jang, G. F.; Kuksa, V.; Filipek, S.; Bartl, F.; Ritter, E.; Gelb, M. H.; Hofmann, K. P.; Palczewski, K. *J. Biol. Chem.* **2001**, *276*, 26148.
(14) Send, R.; Sundholm, D. *J. Phys. Chem. A* **2007**, *111*, 27.
(15) Buchi, G.; Yang, N. C. *Chem. Ind.* **1955**, 357.
(16) Buchi, G.; Biemann, K.; Vittimberga, B.; Stoll, M. *J. Am. Chem. Soc.* **1956**, *78*, 2622.
(17) Marvell, E. N.; Caple, G.; Gosink, T. A.; Zimmer, G. *J. Am. Chem. Soc.* **1966**, *88*, 619.
(18) Marvell, E. N.; Gosink, T.; Caple, G.; Chadwick, T.; Zimmer, G. *J. Org. Chem.* **1972**, *37*, 2992.
(19) Cerfontain, H.; Geenevasen, J. A. J. *Tetrahedron* **1981**, *37*, 1571.
(20) Ramamurthy, V.; Butt, Y.; Yang, C.; Yang, P.; Liu, R. S. H. *J. Org. Chem.* **1973**, *38*, 1247.
(21) Wageningen, A.; Cerfontain, H.; Geenevasen, J. A. J. *J. Chem. Soc., Perkin Trans. 2* **1975**, 1283.
(22) Wageningen, A.; Cerfontain, H. *Tetrahedron Lett.* **1972**, 3679.
(23) de Mayo, P.; Stothers, J. B.; Yip, R. W. *Can. J. Chem.* **1961**, *39*, 2135.
(24) Polyakov, N. E.; Kruppa, A. I.; Bashurova, V. S.; Musin, R. N.; Leshina, T. V.; Kispert, L. D. *J. Photochem. Photobiol., A* **1999**, *128*, 65.
(25) Polyakov, N. E.; Kruppa, A. I.; Bashurova, V. S.; Leshina, T. V.; Kispert, L. D. *J. Photochem. Photobiol. A* **2002**, *153*, 113.
(26) Polyakov, N. E.; Leshina, T. V. *Mol. Phys.* **2002**, *100*, 1297.
(27) Polyakov, N. E.; Leshina, T. V.; Hand, E. O.; Petrenko, A.; Kispert, L. D. *J. Photochem. Photobiol., A* **2004**, *161*, 261.
(28) Mathies, P.; Nishio, T.; Frei, B.; Jeger, O. *Helv. Chim. Acta* **1989**, *72*, 933.
(29) Frisch, M. J.; Trucks, G. W.; Schlegel, H. B.; Scuseria, G. E.; Robb, M. A.; Cheeseman, J. R.; Montgomery, J. A., Jr.; Vreven, T.; Kudin, K. N.; Burant, J. C.; Millam, N. J.; Iyengar, S. S.; Tomasi, J.; Barone, V.; Mennucci, B.; Cossi, M.; Scalmani, G.; Rega, N.; Petersson, G. A.; Nakatsuji, H.; Hada, M.; Ehara, M.; Toyota, K.; Fukuda, R.; Hasegawa, J.; Ishida, M.; Nakajima, T.; Honda, Y.; Kitao, O.; Nakai, H.; Klene, M.; Li, X.; Knox, J. E.; Hratchian, H. P.; Cross, J. B.; Bakken, V.; Adamo, C.; Jaramillo, J.; Gomperts, R.; Stratmann, R. E.; Yazyev, O.; Austin, A. J.; Cammi, R.; Pomelli, C.; Ochterski, J. W.; Ayala, P. Y.; Morokuma, K.; Voth, G. A.; Salvador, P.; Dannenberg, J. J.; Zakrzewski, V. G.; Dapprich, S.; Daniels, A. D.; Strain, M. C.; Farkas, O.; Malick, D. K.; Rabuck, A. D.; Raghavachari, K.; Foresman, J. B.; Ortiz, J. V.; Cui, Q.; Baboul, A. G.; Clifford, S.; Cioslowski, J.; Stefanov, B. B.; Liu, G.; Liashenko, A.; Piskorz; P.; Komaromi, I.; Martin, R. L.; Fox, D. J.; Keith, T.; Al-Laham, M. A.; Peng, C. Y.; Nanayakkara, A.; Challacombe, M.; Gill, P. M. W.; Johnson, B.; Chen, W.; Wong, M. W.; Gonzalez, C.; Pople, J. A. *Gaussian 03*, revision E.01; Gaussian, Inc.: Wallingford, CT, 2004.
(30) Frisch, M. J.; Trucks, G. W.; Schlegel, H. B.; Scuseria, G. E.; Robb, M. A.; Cheeseman, J. R.; Scalmani, G.; Barone, V.; Mennucci, B.; Petersson, G. A.; Nakatsuji, H.; Caricato, M.; Li, X.; Hratchian, H. P.; Izmaylov, A. F.; Bloino, J.; Zheng, G.; Sonnenberg, J. L.; Hada, M.; Ehara, M.; Toyota, K.; Fukuda, R.; Hasegawa, J.; Ishida, M.; Nakajima, T.; Honda, Y.; Kitao, O.; Nakai, H.; Vreven, T.; Montgomery, J. A., Jr.; Peralta, J. E.; Ogliaro, F.; Bearpark, M.; Heyd, J. J.; Brothers, E.; Kudin, K. N.; Staroverov, V. N.; Kobayashi, R.; Normand, J.; Raghavachari, K.; Rendell, A.; Burant, J. C.; Iyengar, S. S.; Tomasi, J.; Cossi, M.; Rega, N.; Millam, N. J.; Klene, M.; Knox, J. E.; Cross, J. B.; Bakken, V.; Adamo, C.; Jaramillo, J.; Gomperts, R.; Stratmann, R. E.; Yazyev, O.; Austin, A. J.; Cammi, R.; Pomelli, C.; Ochterski, J. W.; Martin, R. L.; Morokuma, K.; Zakrzewski, V. G.; Voth, G. A.; Salvador, P.; Dannenberg, J. J.; Dapprich, S.; Daniels, A. D.; Farkas, Ö.; Foresman, J. B.; Ortiz, J. V.; Cioslowski, J.; Fox, D. J. *Gaussian 09*, revision A.02; Gaussian, Inc.: Wallingford, CT, 2009.
(31) Becke, A. D. *J. Chem. Phys.* **1993**, *98*, 5648.
(32) Lee, C.; Yang, W.; Parr, R. G. *Phys. Rev. B* **1988**, *37*, 785.
(33) Vosko, S. H.; Wilk, L.; M., N. *Can. J. Phys.* **1980**, *58*, 1200.
(34) Møller, C.; Plesset, M. S. *Phys. Rev.* **1934**, *46*, 0618.

(35) Head-Gordon, M.; Pople, J. A.; Frisch, M. J. *Chem. Phys. Lett.* **1988**, *153*, 503.
(36) Saebø, S.; Almlöf, J. *Chem. Phys. Lett.* **1989**, *154*, 83.
(37) Frisch, M. J.; Head-Gordon, M.; Pople, J. A. *Chem. Phys. Lett.* **1990**, *166*, 275.
(38) Frisch, M. J.; Head-Gordon, M.; Pople, J. A. *Chem. Phys. Lett.* **1990**, *166*, 281.
(39) Head-Gordon, M.; Head-Gordon, T. *Chem. Phys. Lett.* **1994**, *220*, 122.
(40) Peng, C.; Ayala, P. Y.; Schlegel, H. B.; Frish, M. J. *J. Comput. Chem.* **1996**, *17*, 49.
(41) Peng, C.; Schlegel, H. B. *Israel J. Chem.* **1993**, *33*, 449.
(42) Gomez-Zavaglia, A.; Kaczor, A.; Cardoso, A. L.; Melo, T.; Fausto, R. *J. Phys. Chem. A* **2006**, *110*, 8081.
(43) Gomez-Zavaglia, A.; Kaczor, A.; Cardoso, A. L.; Melo, T.; Fausto, R. *J. Mol. Struct.* **2007**, *834*, 262.
(44) Kaczor, A.; Gomez-Zavaglia, A.; Cardoso, A. L.; Melo, T.; Fausto, R. *J. Phys. Chem. A* **2006**, *110*, 10742.
(45) Pulay, P.; Fogarasi, G.; Pang, F.; Boggs, J. E. *J. Am. Chem. Soc.* **1979**, 2550.
(46) Martin, J. M. L.; Van Alsenoy, C. *GAR2PED*; University of Antwerp: Antwerp, Belgium; 1995.
(47) Frija, L. M. T.; Reva, I.; Ismael, A.; Coelho, D. V.; Fausto, R.; Cristiano, M. L. S. *Org. Biomol. Chem.* **2011**, *9*, 6040.
(48) Lopes Jesus, A. J.; Rosado, M. T. S.; Reva, I.; Fausto, R.; Eusébio, M. E. S.; Redinha, J. S. *J. Chem. Phys. A* **2008**, *112*, 4669.
(49) Rosado, M. T. S.; Lopes Jesus, A. J.; Reva, I.; Fausto, R.; Redinha, J. S. *J. Chem. Phys. A* **2009**, *113*, 7499.
(50) Kaczor, A.; Reva, I.; Warszycki, D.; Fausto, R. *J. Photochem. Photobiol., A* **2011**, *222*, 1.
(51) Breda, S.; Reva, I.; Lapinski, L.; Fausto, R. *J. Phys. Chem. A* **2006**, *110*, 11034.
(52) Krupa, J.; Olbert-Majkut, A.; Reva, I.; Fausto, R.; Wierzejewska, M. *J. Phys. Chem. B* **2012**, *116*, 11148.
(53) Legnani, L.; Luparia, M.; Zanoni, G.; Toma, L.; Vidari, G. *Eur. J. Org. Chem.* **2008**, 4755.
(54) Kaczor, A.; Baranska, M. *Anal. Chem.* **2011**, *83*, 7763.
(55) Kaczor, A.; Turnau, K.; Baranska, M. *Analyst* **2011**, *136*, 1109.
(56) Schlucker, S.; Szeghalmi, A.; Schmitt, M.; Popp, J.; Kiefer, W. *J. Raman Spectrosc.* **2003**, *34*, 413.
(57) Reva, I.; Lopes Jesus, A. J.; Rosado, M. T. S.; Fausto, R.; Eusébio, M. E.; Redinha, J. S. *Phys. Chem. Chem. Phys.* **2006**, *8*, 5339.
(58) Roth, W. R.; König, J. *Liebigs Ann. Chem.* **1966**, *699*, 24.
(59) Dewar, M. J. S.; Healy, E. F.; Ruiz, J. M. *J. Am. Chem. Soc.* **1988**, 2666.
(60) Dewar, M. J. S.; Merz, K. M. J.; Steward, J. J. P. *Chem. Soc., Chem. Commun.* **1985**, 166.
(61) Chantranupong, L.; Wildman, T. A. *J. Am. Chem. Soc.* **1990**, *112*, 4151.
(62) von Doering, W.; Keliher, E. J.; Zhao, X. *J. Am. Chem. Soc.* **2004**, *126*, 14206.
(63) Hayase, S.; Hrovat, D. A.; Borden, W. T. *J. Am. Chem. Soc.* **2004**, *126*, 10028.
(64) Brouwer, A. M.; Jacobs, H. J. C. *Recl. Trav. Chim. Pays -Bas* **1995**, *114*, 449.
(65) Sundaralingam, M.; Beddell, C. *Proc. Natl. Acad. Sci. U.S.A.* **1972**, *69*, 1569.
(66) Cerfontain, H.; Geenevasen, J. A. J. *J. Chem. Soc., Perkin Trans. 2* **1978**, 698.
(67) Cerfontain, H.; Geenevasen, J. A. J.; Vannoort, P. C. M. *J. Chem. Soc., Perkin Trans. 2* **1980**, 1057.
(68) Raynaud, C.; Poteau, R.; Maron, L.; Jolibois, F. *J. Mol. Struct.: THEOCHEM* **2006**, *771*, 43.